Iranian Journal of Hydrogen & Fuel Cell 2(2019) 141-161

Iranian Journal of Hydrogen & Fuel Cell

IJHFC

Journal homepage://ijhfc.irost.ir

Synthesis and Electrochemical Characterization of Graphene-Polyallylamine Nanocomposites as New Supports of Pt Catalyst for Direct Methanol Fuel Cell Application

Maryam Yaldagard*

Department of Chemical Engineering, Urmia University, Iran

Article Information

Article History:

Received:
3 Sep 2019
Received in revised form:
27 Dec 2019
Accepted:
1 Feb 2020

Keywords

Graphene
Polyallylamine
Nanocomposite
Support
Microwave assisted polyol process
Methanol
Fuel cell

Abstract

In this research, nanocomposites of Platinum Graphene-Polyallylamine (Pt/PAA/GNP) were developed to increase the methanol electro-oxidation activity and stability of commercial Pt/C electrocatalyst. After the synthesis process, graphene oxide was functionalized with Polyallylamine via the cross linking approach, then Pt as a catalyst was dispersed on the as prepared support by a novel process, which is a polyol synthesis method assisted by microwaves. X-ray diffraction (XRD) results showed that Pt particles, with a mean particle size of about 6.17 nm, were dispersed on the support. FESEM images showed that the Pt nanoparticles were successfully dispersed on the functionalized graphene nanoplates. Based on the electrochemical properties characterized by cyclic voltammetry (CV), including CO stripping measurements, it was found that the prepared Pt/PAA/GNP electrocatalyst exhibited a comparable activity for methanol oxidation reaction with respect to the commercial one. A significant reduction in the potential of the CO electro-oxidation peak from 0.93V for the Pt/C to 0.89 V for the Pt/PAA/GNP electrocatalyst indicates that there was a significant increase in the CO electro-oxidation activity, which is achieved by replacing the voulcan. Also, the as prepared Pt/PAA/GNP electrocatalyst exhibits high catalytic activity for the MOR in terms of electrochemical surface with respect to Pt/C (40.53 vs 17.61 $m^2/mgPt$), which may be attributed to structural changes caused by the high specific surface area of the PAA modified graphene nanoplates catalyst support. Moreover, chronoamerometry results showed that in the presence of methanol, the Pt/PAA/GNP electrocatalyst still maintains a higher current density than Pt/C.

1. Introduction

A direct methanol fuel cell (DMFC) is an electrochemical device that converts chemical energy into electricity using methanol and oxygen as anode and cathode reactants, respectively. The oxidation of methanol has been thoroughly studied for many years and the mechanism is now well established.

*Corresponding Author's Fax: +98-4432775660
E-mail address: m.yaldagard@urmia.ac.ir

doi: 10.22104/ijhfc.2020.3794.1195

It has been reported that the dissociative adsorption of methanol on Pt-based catalysts occurs via the formation of irreversibly adsorbed CO species (a reaction intermediate), either linearly bonded or bridge bonded to the Pt surface[1]. The detailed reaction mechanism of methanol oxidation on a Pt electrode is shown in Fig. 1 [1]. The overall oxidation reaction of methanol involves six electrons and one water molecule,

$CH_3OH+H_2O \rightarrow CO_2+6H_{aq}^{+}+6e^{-}$ (anode reaction)

$1.5O_2+6H_{aq}^{+}+6e^{-} \rightarrow 3H_2O$ (cathode reaction)

Corresponding to the anode potential Ea = 0.016V (under standard conditions) versus SHE, results in the equilibrium standard electromotive force of 1.213 V for a DMFC. The overall reaction of the cell is:

$CH_3OH+1.5O_2 \rightarrow CO_2+2H_2O$ (overall reaction)

A direct methanol fuel cell is the most promising candidate for portable power applications due to its advantages of high power density amount, good environmental aspects, easy storage of fuel, and low operational temperatures [2, 3]. Currently, Pt is the most widely used catalyst in DMFC in both anode and cathode sections. However, it suffers from high cost, low kinetics of methanol oxidation, and CO poisoning caused by methanol crossed–over from the anode [4]. From a commercial point of view, DMFCs have been developed to overcome the obstacles of high catalyst cost caused by the exclusive use of platinum and platinum-based electrocatalysts in both the oxidation of methanol and the reduction of oxygen at the fuel-cell electrodes of methanol [5, 6]. Electrochemical oxidation of methanol has been attracted notable interest due to the great potential of DMFC. Several strategies have been explored with the purpose of reducing the cost and increase the performance of a DMFC. Two active approaches in the reduction of Pt usage in DMFC catalyst are: (i) Reducing Pt usage by utilizing an alloy with other transition metals, Ru is a most promising and is used extensively in Pt catalysts (ii) Improving the performance of carbon-based electrocatalyst supports and exploring novel non-carbonaceous electrocatalyst support materials by employing nanotechnology to increase the surface area and other properties. A number of investigations on nanostructure supported Pt-based

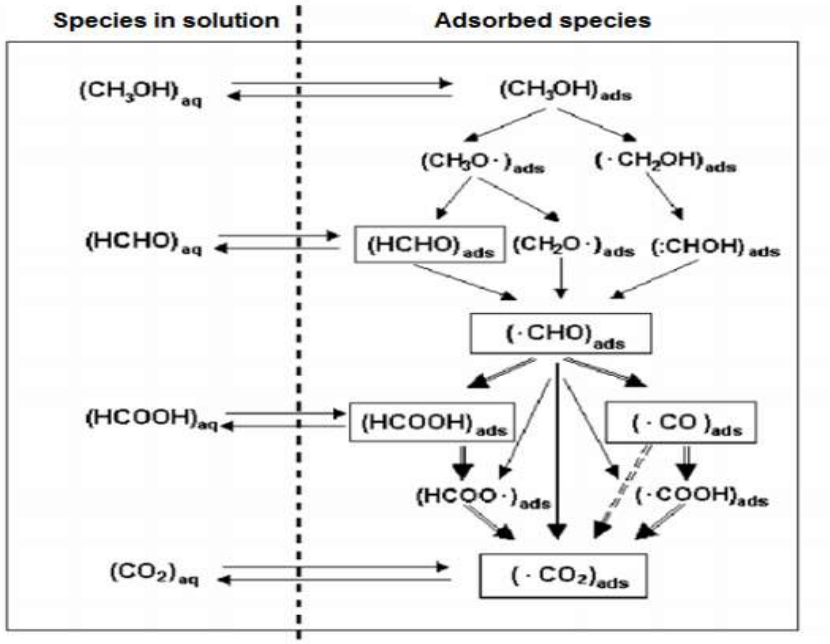

Fig. 1. Detailed reaction mechanism of methanol oxidation on a Pt electrode [1].

nanoparticles as electrocatalyst have received greater attention owing to their synergistic effects that enable the improvement of their catalytic activities in the methanol electrochemical oxidation reaction [7-11]. On the other hand, the support itself has an important influence on the catalytic efficiency of Pt catalysts. In addition to their abundance and stability, carbon based materials have demonstrate unique properties and promising applications. Different arrangements of carbon atoms have resulted in many allotropes like carbon nanofibers (CNFs), carbon nanotubes (CNTs), and graphite. The elusive two-dimensional form of carbon is called graphene, is probably the best-studied carbon allotrope theoretically. Carbon black (Vulcan XC-72, Cabot Crop.) is widely used as supporting material for Pt because of its high surface area and low cost. However, the inadequate performance of Pt/C as well as the lack of long term stability of carbon black under fuel cell operation still calls for new and improved materials. Recently, carbons with different structures, such as nanotubes and nanofibers, have been studied extensively as electrocatalysts supports due to their unique electric and micro-and macrostructure properties [12-14]. Since the discovery of single-layer graphene in 2005 [15, 16], it has attracted interest from both experimental and theoretical scientific communities [17].

Graphene, a one-atom thick layer of sp2 carbon atoms tightly packed into a honeycomb lattice, has attracted tremendous scientific attention in recent years. This amazing two –dimensional form of carbon exhibits unique electrical, thermal, mechanical, and other characteristics. The novel characteristics of graphene have captured great attention in energy technology applications. With better understanding of their excellent physical and chemical properties, graphene has raised a new wave of research worldwide and become a star in the areas of nanoelectronics, sensors, nanocomposites, batteries, supercapacitors, and hydrogen storage. Owing to its high surface areas (theoretical specific surface area of 2620m^2g^{-1}), superior electric conductivities, and outstanding mechanical properties, graphene has a potential application as a heterogeneous catalyst support in DMFCs. Pioneer studies have pointed out that metal nanoparticles supported on graphene nano sheets provide excellent catalytic activity [11, 18-21]. Several investigations have been carried out to produce graphene nanosheets in bulk quantity via the chemical reduction of graphite oxide (GO) in solution [22-25]. Since abundant functional groups (C-OH , C-O-C and HO-C=O) on the surfaces of GO can be used as anchoring sites for metal nanoparticles [26], it is possible to use them as supports to produce graphene-nanoparticle hybrids. A combination of graphene and functional groups may lead to materials with interesting properties for a catalyst in DMFC applications, and they are specifically expected to enhance electrocatalytic activity. Many efforts, such as graphene nitrogen doping [27-30], long chain polymer doping [31, 32], conducting polymers [33-36], graphene functionalized with chelating groups [37], graphene-CNT hybrids [38-40], and graphene oxide metals have been considered over past several years to further modulate the properties of graphene [41-43]. Polyallylamine (PAA) is a long alkyl chain with several reactive amine groups that can easily react with oxygen functional groups of the graphene oxide sheets. Polyallylamine is a linear cationic polyelectrolyte with primary amine groups on the chain and is widely used as a binder for attaching nanoparticles on the surface of carbon nanotube (CNTs) electrodes [44-46]. Recently, PAA has been reported as a molecular binder , and a modified PAA–CNTs was developed to enhance the interaction strength between the nanotubes and associated species [47]. Moreover, in experiments conducted by Sungjin Park et al. , PAA has been reported as a cross linked material, and a PAA modified graphene exhibited excellent mechanical stiffness and strength [48]. Similar results have been reported by Satti and coworkers [49].

Microwave-assisted synthesis is an emerging technology using the ability of microwave heating

to accelerate chemical reactions. Some liquids and solids are able to transform electromagnetic energy into heating. Microwave-processing of materials is fundamentally different from conventional processing due to its different heating mechanism. In a microwave oven, due to the interaction of micro-waves with the material, the heat is generated within the sample itself. In conventional heating, the heat is generated by heating elements and then it is transferred to the sample surface [50]. The greatest advantage of microwave irradiation is that it can heat a substance uniformly through a glass or plastic reaction container, leading to a more homogeneous nucleation and a shorter crystallization time compared with those for conventional heating. This is beneficial to the formation of uniform colloidal materials. Specifically, using microwaves as a heat source in a chemical process leads to rapid volumetric heating, and is capable of improving the reaction rates, yields, and uniformity of products [51]. Microwaves have been used for processing advance materials [50].

In the present study, for the synthesis of Pt nanocrystals on PAA functionalized graphene via cross linking, the polyol process has been used in preparing colloidal metal particles [52]. The microwave procedure, as a novel technique, was adopted in order to avoid the agglomeration of the metal particles at high temperatures. The present microwave assisted polyol process is simple, practical, and effective for rapid synthesis of a high dispersed loading Pt-based electrocatalyst. The graphene support is also a microwave-sensitive material, which is believed to play an important role in the acceleration of the metal reduction. The quite short metal reduction process is attractive and interesting from an economic point of view. Indeed, the aim of this study is to reduce the cost of fuel cell catalysts through improvement of Pt nanoparticles dispersion using a high-surface area support modulated via a functionalized group of PAA. It must to mentioned that the results of this paper are in good accordance with others [48, 49, 53-55].

2. Experimental Procedure

2.1. Materials

High-purity graphite powder (99.9999%, 200 mesh) was purchased from Alfa Aesar. Chemicals $H_2PtCl_6 \cdot 6H_2O$ (99.95%), Na_2NO_3, $KMnO_4$, and H_2O_2 were obtained from Sigma-Aldrich. All solvents, including H_2SO_4, 2-propanol, were used as received from Sigma-Aldrich without further purification. Polyallylamine (PAA) (Sigma-Aldrich, 20 wt% aqueous suspension of PAA with Mw = 17,000), Nafion® solution (Ion power Inc, USA 5 wt%), and Pt/C (20wt%) were bought from the Fuel Cell Earth Company. High purified N_2 (99.9995%), CO (99.99%), and O_2 (99.999%) gases were purchased from Canadian Sigma Inc. Water was purified by a Milli-Q water purification system was used throughout the experimental work.

2.2. Methods

2.2.1. Preparation of Graphene Oxide (GO)

In a typical synthesis process, natural graphite powder was oxidized to graphite oxide by a modification of Hummers and Offenman's method [56]. In brief, 2 g graphite powder and 1g sodium nitrate were poured into 90ml concentrated H_2SO_4 in an ice bath condition. Then 6g $KMnO_4$ was gradually added. The mixture was stirred at 35±5 ℃ for 8h. Then 200ml deionized water (DI) was added and the temperature was kept at 95±5 ℃ for 30 min. Finally, it was diluted with 400 ml DI. After that, 5% H_2O_2 was added into the solution until the colour of the mixture changed from brown to peril yellow. The solution was filtrated via vacuum buchner filtration and the filter cake dispersed in DI by means of ultrasonic bath. The mixture was washed with 1:20 HCL solution and water (in order to remove metal ions) by repeated centrifugation (at 11000 rpm for 20 min) to a PH value of 7 and then dried in a vacuum oven at 60 ℃ for 24h.

2.2.2. PAA modified graphene oxide nanosheets

Colloidal dispersions of individual graphene oxide sheets in purified water (30 mg GO/10 mL water) were prepared with the aid of ultrasonic batch. Adding polyallylamine (PAA) to the aqueous suspension of the graphene oxides immediately generated agglomerates. It was then ultrasonication for an additional 2 h under diluted condition (1 mg GO/5 mL water) and then stirred in a magnetic stirrer for 12h, affording the homogeneous colloidal suspension of PAA-modified graphene oxide sheets. The solution was filtered via a dead-end set-up using N2 gas through a home-made ultrafilter and further washed with warm water. The residue was dried in a vacuum oven at 45℃ for 8h [48].

2.2.3 Microwave assisted polyol synthesis of Pt/ PAA modified graphene nanoplates

Pt /PAA modified-graphene nanoplates were prepared by microwave heating of an ethylene glycol (EG) solution of hexacholoroplatinic acid precursor salts. As a typical process for the synthesis of Pt/ PAA modified-graphene nanoplates with the Pt loading of 10 wt%, 12.5 mg $H_2PtCl_6.6H_2O$ was mixed with 25 ml of EG. Then the pH value of the solution was adjusted to about 12 using HCL and NaOH. Four mg of PAA modified-graphene nanoplates were uniformly dispersed in the mixed solution by ultrasonic bath. Subsequently, the solution was directly (in sample cups) placed in a microwave oven and irritated at 1000W for 3 min at 160◦C. The resulting suspension was centrifuged at 11000 rpm (at SW14, Froilabo) for 20min and then the residue was washed with acetone. The recovered solid product was dried at 50◦C overnight in a vacuum oven. Pt/C was also employed as a reference electrocatalyst for comparison. A schematic of the experimental procedures used in this study for the preparation of Pt/PAA/GNPs is demonstrated in Fig. 2.

2.2.4 Preparation of electrode

The working electrode was glassy carbon (GC) with a diameter of 2 mm covered with a thin layer of nafion-impragnated catalyst. The thin film was prepared with about 5 mg of the as synthesized catalyst powder mixed in 3.98ml DI water,, 1ml isopropanol, and 20 microliter 5%wt nafion solution. The catalyst ink was ultrasonicated for 1h. An appropriate amount of the resulting suspension was pipetted onto a GC electrode several times after drying the electrode in air and subsequently weighted until the loading of

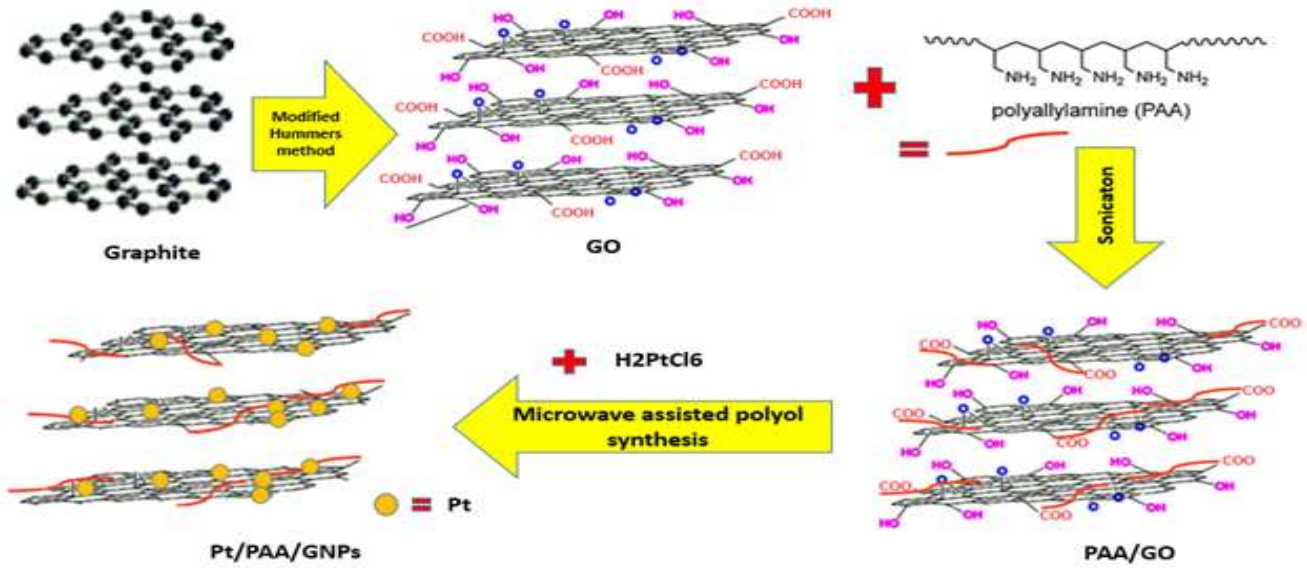

Fig. 2. A schematic of the experimental procedures used in this study for the preparation of Pt/PAA/GNPs.

0.4 mgcm^{-1} was attained. Prior to use, the electrode was polished using aqueous alumina suspensions with successively smaller particle sizes between 1μm and 0.05 μm on felt polishing pads. In order to remove any trace impurities after polishing the electrode was ultrasonicated for 10 min in ethanol and DI water. Pt foil served as a counter electrode while KCl saturated Ag/AgCl was used as a reference electrode. All potentials in this report are quoted versus KCl saturated Ag/AgCl. A CV test was conducted at 50mv/s in a solution of 0.5 M H_2SO_4 solution saturated with high purified nitrogen gas (99.9995%) with 2M methanol, potential ranging from -0.24 to 1.2V .

2.3 Characterization and Measurements

Fourier transform infrared (FTIR) measurements were recorded on a WQF-510A/520 FTIR spectrometer. Spectra were obtained in the range of 500-3500 cm^{-1}.
The morphology, topography, and other structure studies of the graphene sheets was examined by an atomic force microscope (AFM, model Nanosurf easy scan2) using contact mode.
Field emission–scanning electron microscopy (FE-SEM) characterization and Energy dispersive X-ray (EDX) spectroscopy coupled with a scanning electron microscopy SEM MAG100.00kx with a silicon detector was performed at 15 kv.
The crystal structure of the catalyst was measured by X-ray diffraction at 25 ℃ with an X'Pert Pro MPD model (PANalytical) Diffractometer using Cu Kα (λ=0.15406nm) radiation generated at 40KV and 40 mA with high resolution (0.001º). The 2θ angular regions between 10 º and 90 º were recorded with a step size of 0.039 (at scan step time of 108.12s) with continues scanning. The analysis of phase was conducted by X'Pert Highscore plus software from the composite.
Electrochemical reactivity of the nanocomposite and methanol oxidation and CO stripping experiments as well as impedance measurements were measured in the three-electrode cell at a Iviumstat potensiostat/ galvanostat XR electrochemical interface system.

3. Result and Discussion

3.1 Physical characterization

3.1.1 Topographical characterization of PAA-modified graphene oxide nanoplates via the cross linking process using atomic force microscopy (AFM)

The PAA-modified graphene nanoplates were analyzed by atomic force microscopy to determine its thickness and lateral size. Fig. 3 shows an AFM image of PAA-modified graphene nanosheet surfaces along with the corresponding height profile produced by sonication. The zoomed image of graphene nanoplates and corresponding line scan are also shown in Fig.3, from which the topographic height of the graphene nanoplates is measured to be about 19-156.2nm, indicating few-layered graphene nanoplates [57, 58].

3.1.2 FTIR analysis of GO and PAA-modified graphene oxide nanoplates via cross linking

Fig. 4 indicates the FT-IR spectra of graphene oxide (GO) and PAA functionalized graphene oxide by sonication. Absorption peaks at 2989, 1643cm^{-1} correspond to C-H and C=C modes in GO, while two new peaks, one peak at 1758cm^{-1} (C=O) are from the carbonyl and carboxylic groups and the other peak at 1045cm^{-1} (C–O) are from carbonyl, carboxylic and epoxy groups, which confirms the presence of oxygen-containing functional groups. After the modification of graphene oxide sheets with PAA, the relative intensity of the epoxy C-O stretch of the PAA-modified graphene oxide paper at 1222cm^{-1} significantly decreased. As graphene oxide has been found to contain reactive epoxy groups, its exposure to amine groups would lead to a ring-opening reaction of the reactive three-membered epoxide ring, creating new C-N bonds. The ring-opening reaction of the epoxy group from the attack of nucleophiles, such as amine groups, has been well established [59]. The increase of the peak intensity at 1500cm^{-1}, which corresponds to a stretching of

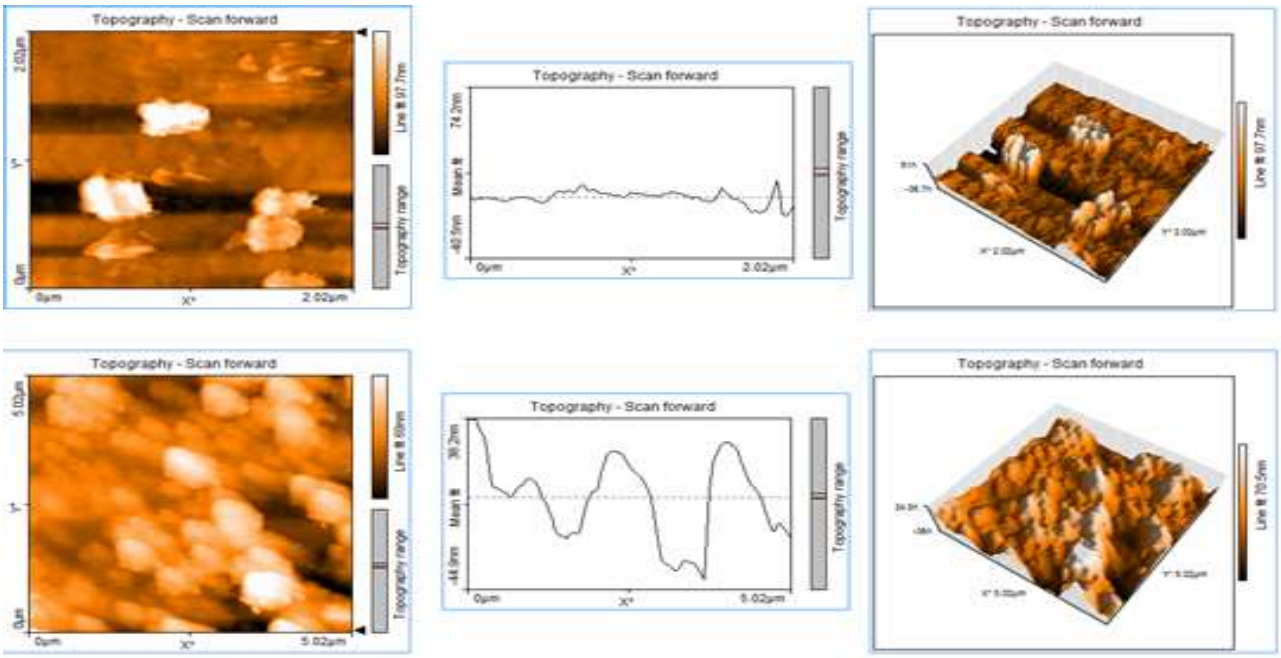

Fig. 3. AFM topography images of (top) graphene oxides nanoplates (bottom) PAA-modified graphene nanoplates via cross linking. Next to the images are a line scan taken horizontally through the image as marked with an arrow, from which the height of a graphene nanoplates were determined.

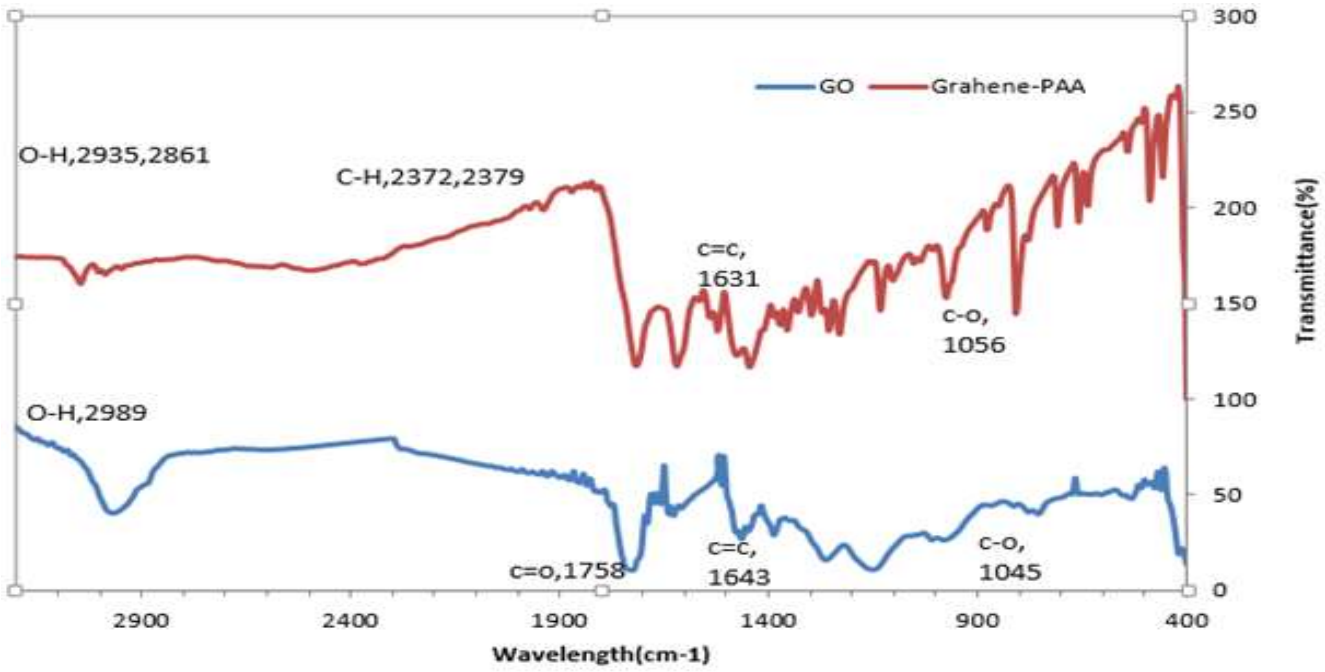

Fig. 4. FTIR analysis of GO and PAA-modified graphene nanoplates via cross linking

the new C-N bonds and possibly residual PAA, was observed in the FT-IR spectra of air-dried PAA-modified graphene oxide paper samples. In addition, significantly decreased C-O stretches and shifted carboxy C-O stretches were observed after PAA modification of graphene oxide sheets. This could be interpreted as evidence that carboxylic acid groups interact with amine groups [60].

3.1.3 Raman characterization of GO and PAA-modified graphene oxide nanoplates via cross linking

Raman spectroscopy is a useful tool to characterize graphitic materials, especially for distinguishing graphene and graphene oxide. It is a non–destructive technique which provides detailed structure information such as the disorder and defect structures of graphene [61]. The Raman spectrum of graphene is characterized by three main features due to the change in electron bands: the G mode related to the vibration of sp2–bonded carbon atoms in two-dimensional hexagonal lattice (usually observed at about 1575cm^{-1}), the D mode arising from the doubly resonant disorder-induced mode and related to defects (about 1350cm^{-1}), and the symmetry or allowed 2D overtone mode (about 2700 cm^{-1}) bond which is at almost double the frequency of the D band and originates from second order Raman scattering process [25, 62-68]. As the structure changes from graphite to nanocrystalline graphene in graphene studies, the ratio between the peak intensity of the D and G line, ID/IG, changes inversely with the size of the crystalline grains or interdefect distance [69]. The higher ID/IG intensity ratio of the sample can be used as an evidence for the structure order.

Fig. 5 shows the typical Raman spectra of graphene oxide and the PAA-modified graphene nanoplates via cross linking method. GO displays two prominent peaks, which correspond to the well-documented G and D bands. The GNP displays three main featured peaks namely the G-band, D-band, and 2D band at 1585.66cm^{-1}, 1311.30 cm^{-1}, and 2611.92cm^{-1}, respectively. For GNPs, the G band moved from 1586cm^{-1} of graphene oxide to 1585cm^{-1} which is closer to the value of the pristine graphite, confirming the reduction of graphene oxide by sonication. It is well documented that the oxygen functional groups in graphene oxide can be removed and a conjugated graphene network (sp2 carbon) will be reestablished in the modified graphene cross linked by PAA. The reestablished graphene network usually has a smaller average size than the original graphene oxide, which consequently leads to the increase of intensity ratio (ID/IG). The ID/IG ratios for modified graphene cross linked by PAA are about 1.71, which are larger than GO (by about 1.34). Thus, it is further concluded that graphene oxide in modified graphene cross linked by PAA has been well deoxygenarated and reduced to graphene.

It must be mentioned that in this figure no peak corresponding to PAA was observed, the same results have been reported by other researchers [47, 70]. Shape and position of the 2D band are the key factors indicating information and the layer number of the graphene sheets. From Fig .5, the observed 2D band of modified graphene cross linked by PAA with a nearly symmetrical shape was centered at 2611.92cm^{-1}, suggesting formation of single or bilayer GNPs. Therefore, Raman spectroscopy confirms that modified graphene cross linked by PAA is greatly exfoliated and the D band related to more defects arises mostly from the edges and fractures present in the GNPs. This is further proven with a FE-SEM observation and roughness measurements. The average roughness of this nanoplates is 242.01nm, which is related to the surface of the folded sheets. Relatively high defect produced graphene nanoplates on the gas diffusion substrate are an ideal matrix for active sites as support for electrocatalyst deposition, which can act as nucleation centers as well as uniform gas distribution for good management of reactions.

3.1.4 XRD pattern characterization of prepared Pt/PAA/GNP electrocatalyst

Fig. 6 shows the X-ray diffraction patterns of the Pt/PAA/GNP and Pt/C electrocatalysts, which reveal the diffraction peaks of both carbon and platinum. The sharper and narrow diffraction peak at $2\theta=26.8^{o}$ (002) is characteristics of the parallel graphene layers in the Pt/PAA/GNP electrocatalyst and indicate a highly graphitic and crystallinity ordered structure of GNP in planes of (002), while the strong peak at about $2\theta=25.2^{o}$ in the Pt/C electrocatalyst can be attributed to XC-72 carbon present in the commercial Pt/C from Fuel Cell Earth. The peaks at the Bragg angles of 39.87^{o}, 46.38^{o}, 68.70^{o}, 81.47^{o} and 85.92^{o} correspond to the (111), (200), (220), (311) and (222) crystalline plane diffraction peaks, respectively. All peaks can be indexed as the Pt face centered cubic (fcc) phase. In addition to the main characteristic peaks of the graphite and Pt fcc structure, several other weak reflections (represented by an asterisk in Fig. 5) were found in both of the electrocatalyst and are related to the PAA. The peaks of the prepared Pt/PAA/GNP electrocatalyst are sharper than those of Pt/C electrocatalyst, indicating that they have larger particle sizes than the commercial supported

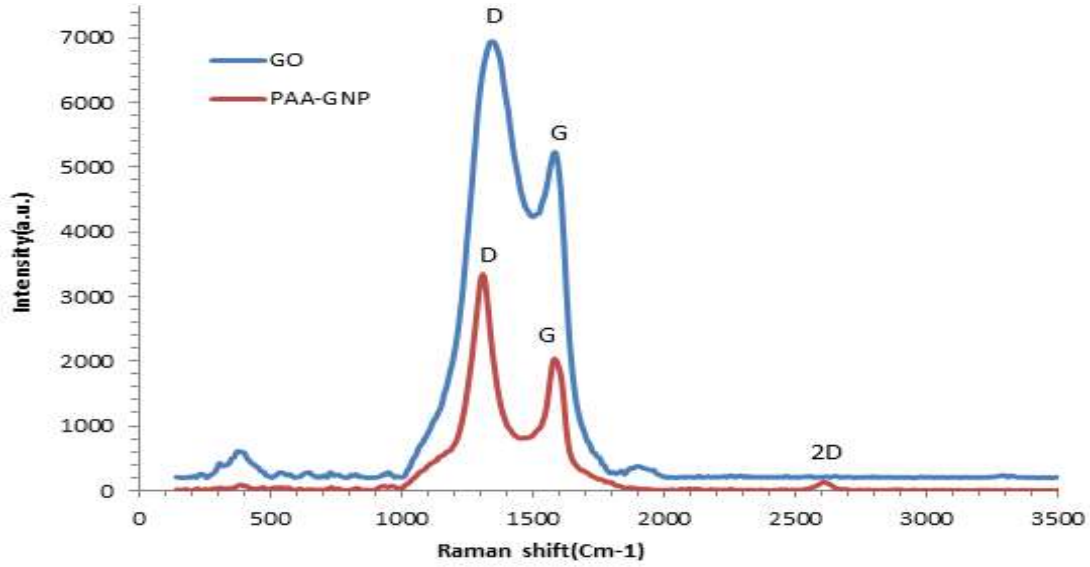

Fig. 5. Raman characterization of GO and PAA-modified graphene oxide nanoplates via cross linking.

platinum. The average size of Pt particles were calculated from the Debby-Scherrer equation using the full width at half maximum (fwhm) of the (111) reflection [71]. Pt (111) plane was selected for Scherrer analysis because it has the highest intensity value. The corresponding calculated nanoparticles size were 6.17 and 3.4nm for Pt/PAA/GNP and Pt/C, respectively.

3.1.5 Morphology and Structural Characterization of GO and Pt/PAA/GNP

Fig. 7 shows the SEM surface morphology of the prepared (a) graphene oxides by the modified Hummer and Affman method, (b) PAA modified graphene nanoplates, and (c) Pt nanoparticles synthesized on a support by the microwave assisted polyol method. A relatively high density of in situ reduced graphene nanoplates is seen in Fig. 7a. As can be seen in Fig. 7b, the entire surface of the graphene nanoplates are decorated by Pt nanoparticles. Furthermore, the FESEM images show that the crystals of Pt are spherical and clean. As shown in Fig. 5b, the spherical platinum nanoparticles on the PAA modified graphene nanoplates are more or less are uniform and well distributed.

Fig. 8 shows the typical EDS pattern of a Pt/PAA/GNP electrode. It turns out that the prepared electrode contains both of Pt and Co elements. The EDS pattern shows that Pt, C, N and O are the major element of the spectra. The C signal comes from the graphene nanoplates and Nafion solution. Oxygen, F and a small part of S are also derived from Nafion. In addition to Pt and C, the elements of Si, Au, and K were also detected. The strong peak of Si is because of the silicon substrate used in FESEM analysis. The relatively small amount of K observed in the EDS image is essentially from the KCl electrolyte used in the plating bath. The element Au belongs to the Au target from the sputtering chamber used in FESEM chracterization. As it is represented in this table, the amount of Pt loaded on the graphene cross linked PAA can be evaluated quantitatively as 9.73%, which is very nearly to the tehoritical value of 10 wt.%.

Table 1 Composition of Pt/ PAA/GNP Electrocatalyst

Element	Weight%
C	66.38
O	13.19
Cl	0.58
N	6.29
Si	0.98
Na	0.95
K	0.83
Au	1.07
Pt	9.73

3.2 Electrochemical measurements

3.2.1 Electrochemical activity of electrocatalysts

To evaluate the electrochemical characteristics of the prepared electrocatalysts, the cyclic voltammetry tests

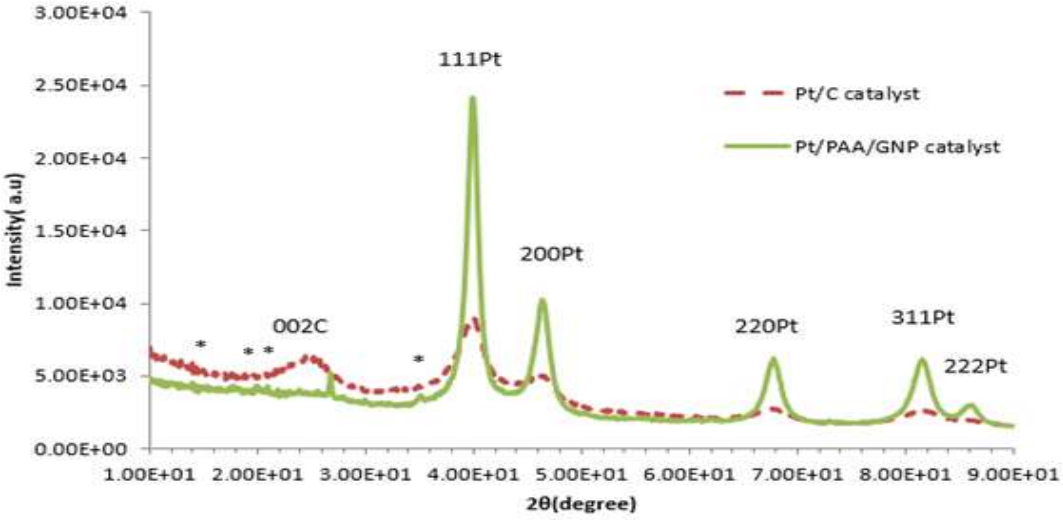

Fig. 6. XRD pattern of prepared Pt/PAA/GNP and Pt/C electrocatalysts.

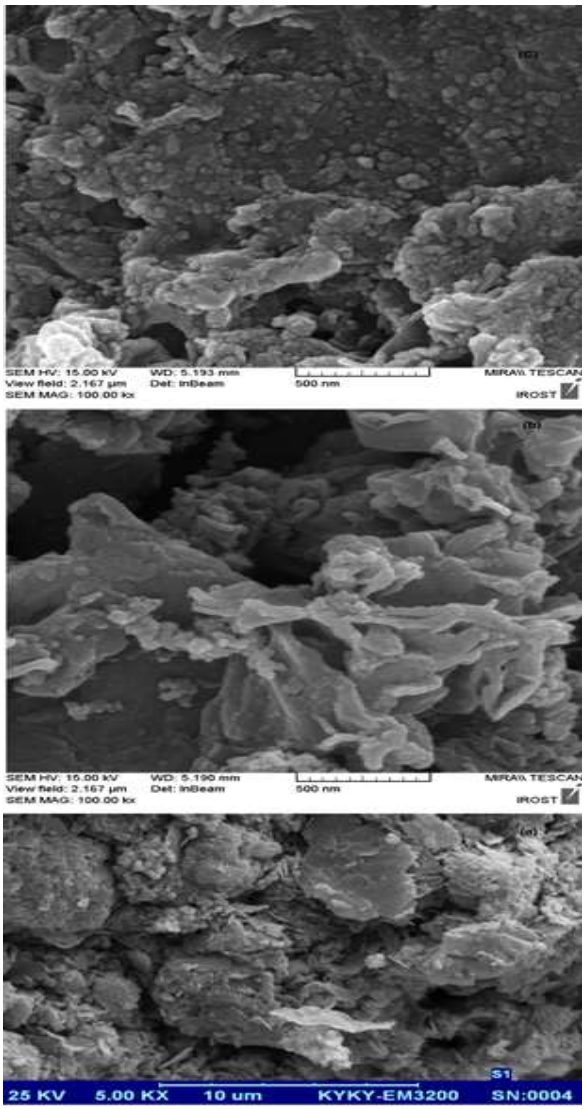

Fig. 7. FE-SEM images of the a) graphene oxides, b) PAA modified graphene nanoplates, and c) Pt nanoparticles synthesized on a support by the microwave assisted polyol method.

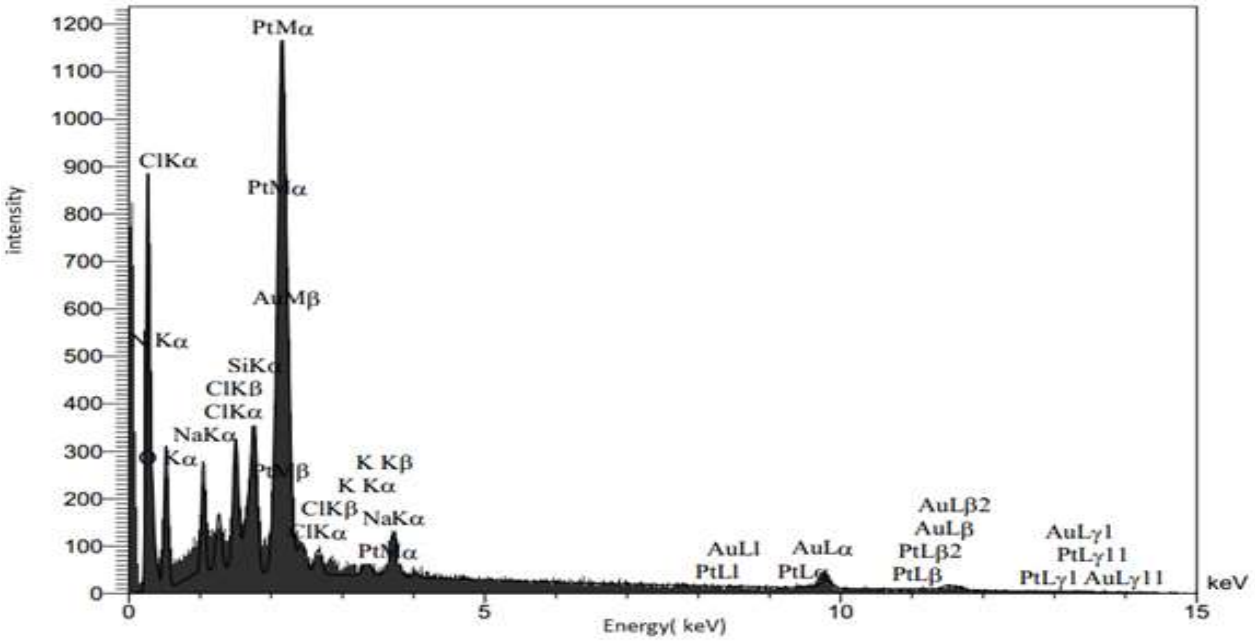

Fig. 8. EDX pattern of Pt/ PAA/GNP.

were carried out using a glassy carbon electrode with the same loading as Pt covered with a Nafion-bonded catalyst layer. Fig. 9 shows the cyclic voltamograms of the prepared electrodes using a potentiostat/ galvanostat, and the calculated electrochemical surface areas (according to supplementary data) are listed in Table 2. As it is shown, the electrochemical surface area increased by platinum nanoparticles supported on the PAA functionalized graphene, indicating that a higher activity achievement by the modified support. Conversely, the specific area decreased mainly because of the increased particle size value of Pt/PAA/GNP with respect to commercial Pt/C. However, the highly active Pt/ PAA/GNP electrocatalyst provided the reasonably high utilization efficiency (89%) of Pt despite its relatively large overall particle size.

Generally, the electrochemical surface area of electrocatalysts increase with a decrease in particle size. However, in this case, the higher electrochemical surface area of the Pt/PAA/GNP electrocatalyst cannot be ascribed to a particle size effect, being the particle size of Pt/C is smaller than those of the Pt/PAA/GNP materials. Our hypothesis is that the promoted electronic conductivity is responsible for the enhancement of the electrochemical surface area. Also, it is believed that the incorporation of PAA into graphene can largely improve its electrochemical activity, showing the Pt/PAA/GNP electrocatalyst is state of the art. In spite of all the mentioned above, the Pt/PAA/GNP electrocatalyst produced in this study has the smallest specific area, due to the particle size effect, as illustrated in Table 2. The XRD characterization showed the largest particle size for the Pt/PAA/GNP electrocatalyst, clearly denoting a lower specific area (see supplementary data), which supports that the specific surface area is dependent on the particle size.

3.2.2 Performance evaluation of catalyst by the methanol oxidation reaction (MOR) and CO tolerance

Fig. 10 displays the cyclic voltammograms for the Pt/PAA/GNP and commercial Pt/C electrocatalysts recorded in 0.5M H_2SO_4+1M CH_3OH at a scan rate of 50mV s^{-1} . It is well known that the activity of the catalyst is mainly evaluated by parameters of onset potential, peak potential, and current density. In the voltammogram, the anodic forward scan is attributed to methanol oxidation, forming Pt-adsorbed carbonaceous intermediates, including CO and CO_2. The backward oxidation peak is ascribed to the additional oxidation of the adsorbed carbonaceous species to CO_2. As can be seen, the first methanol electro-oxidation peak potential in the forward scan is located around 0.7V for Pt/PAA/GNP, which is slightly lower than that of the Pt/C (0.74V), implying higher activity for methanol oxidation on the Pt/

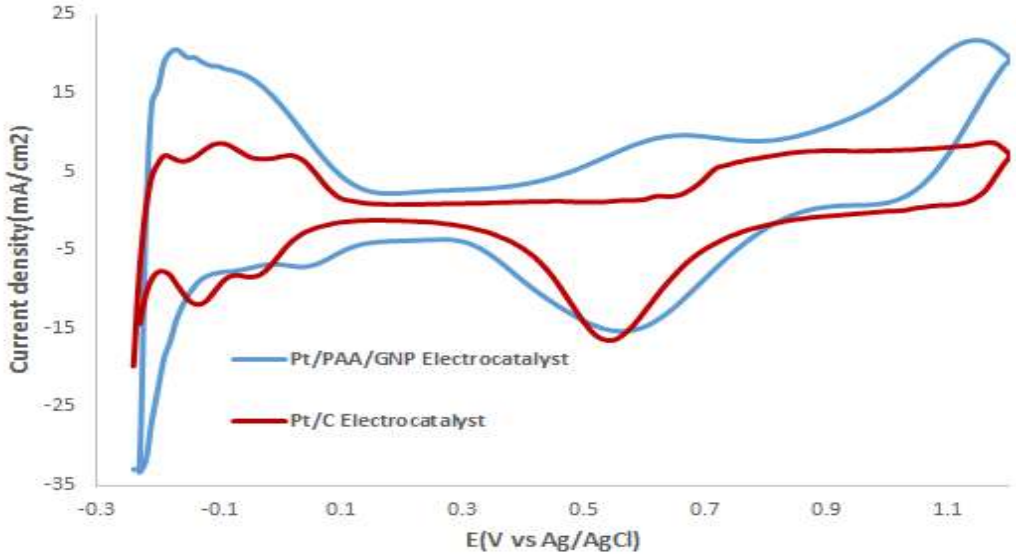

Fig. 9. Cyclic voltamograms of Pt/ PAA/GNP and Pt/C in 0.5M H_2SO_4 solution scan rate: 50mV s^{-1}.

Table 2. Electrochemical Surface Area, Specific Area and Utilization Efficiency of Pt/PAA/GNP and Pt/C Catalysts in a N_2 Saturated Solution of 0.5M H_2SO_4

Catalyst	S_{ESA} (m^2 Pt)/(mgPt)	S_{CSA} (m^2 Pt)/(mgPt)	γ_{Pt} (%)
Pt/PAA/GNP	40.53	45.44	89
Pt/C	17.61	82.26	26

PAA/GNP electrocatalyst. Also, the Pt/PAA/GNP electrocatalyst exhibits an especially higher current density of 32.425mA mg_{Pt}^{-1} at a lower onset of 0.18V potential compared with that of 19.85mA mg_{Pt}^{-1} and 0.29V for the Pt/C electro catalyst, indicating that Pt/PAA/GNP exhibits higher catalytic activity for methanol electro-oxidation than Pt/C. In addition, the observation of much higher I_f/I_b values on Pt/PAA/GNP (2.04 vs 1.51 on Pt/C) implies that methanol molecules are more effectively oxidized on Pt/PAA/GNP during the forward potential scan, generating relatively less poisoning species compared with commercial Pt/C. This could be due to the conducting nature of PAA-modified graphene oxide [72] which enhances proton and electron transport within the anode electrocatalyst. Also, in the cross linking of PAA to graphene structure, PAA acts as an interface and increasing the metal dispersion, like Pt, on the support and improves the electrocatalytic properties in this way.

It was well known that graphene contains some defects such as the oxygen-containing functional groups on the surface. Graphene sheets with these defects are easily to be oxidized and are unstable under fuel cell operation [31]. N-doping of graphene can fix these defects by removing these oxygenated groups, thereby enhancing the stability and conductivity of graphene. In addition, N-doping not only modifies the graphene surface by forming the nitrogen functional groups, but also it can also changes its electronic structures [73]. Moreover, N-doping is also contributing contributes to the effective immobilization of metal nanoparticles by strengthening the metal support interaction [74, 75]. So, from the above obtained results it is concluded that the Pt/ PAA/GNP electrocatalyst showed the better performance for methanol electro-oxidation than Pt/C. The reason is that the Pt/ PAA/GNP has a much larger electrochemical surface area than Pt/C due to the its enhanced conductivity than Pt/C as shown in Fig. 9.

Further investigation was made into the transport behavior of methanol on the nanocomposite electrocatalyst at different scan rates. Ffrom Ffig. 11 , it can be seen that the peak current density of methanol oxidation increases with the increase of scan rates and the peak potential has almost have no significant change. The inset in Ffig. 11 indicates that the anodic peak current densities are linearly proportional to the square root of the scan rate, which reveals that the electrocatalytic oxidation of methanol on the nanocomposite electrocatalyst is a

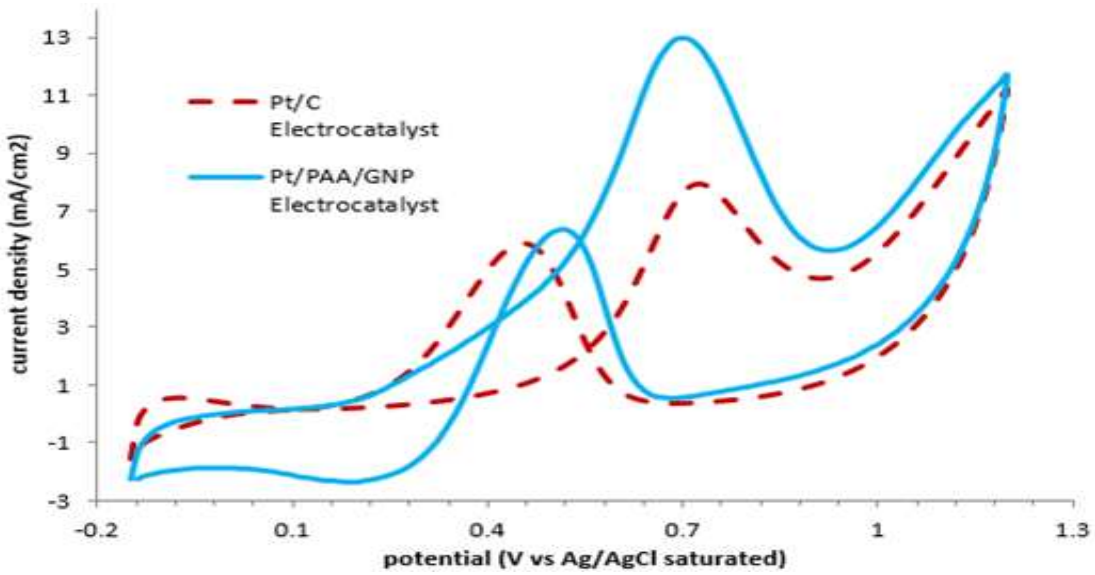

Fig. 10. Cyclic voltamograms of methanol oxidation of Pt/PAA/GNP and Pt/C in 0.5M H_2SO_4+1M CH_3 OH solution scan rate: 50 mV s^{-1}

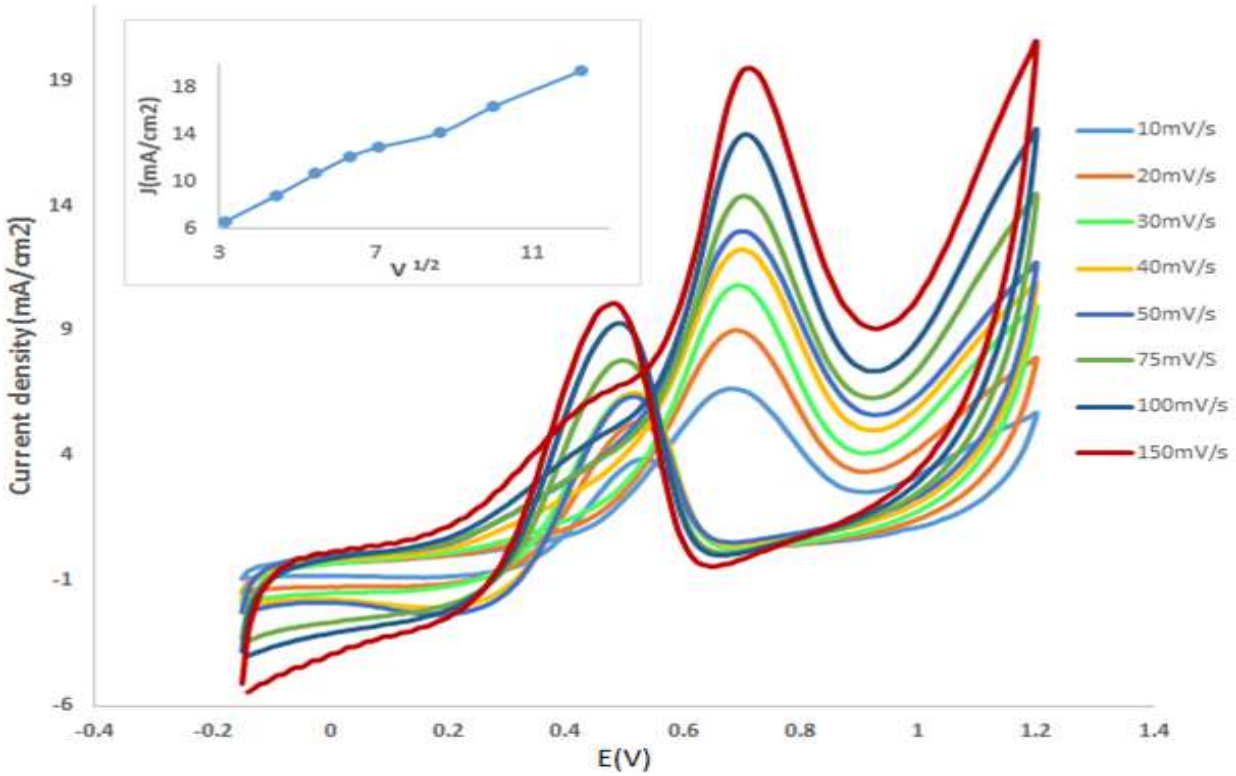

Fig. 11. The anodic peak current densities of Pt/ PAA/GNP in 0.5M H_2SO_4+1M CH_3OH solution at different scan rates. The inset shows the dependence of the anodic peak current densities on the square root of scan rates.

diffusion-controlled process [76].

As CO species are the main poisoning intermediates during the methanol electro-oxidation, a good electrocatalyst for methanol oxidation should possess excellent CO electro-oxidation ability and high tolerance, which can be evaluated by CO stripping voltammetry. If a catalyst has higher CO oxidation ability and tolerance for CO poisoning, it can oxidized more CO or oxidized CO more quickly at lower potential.

Fig. 12 shows the CO stripping voltammograms of Pt/PAA/GNP and Pt/C, which were performed by

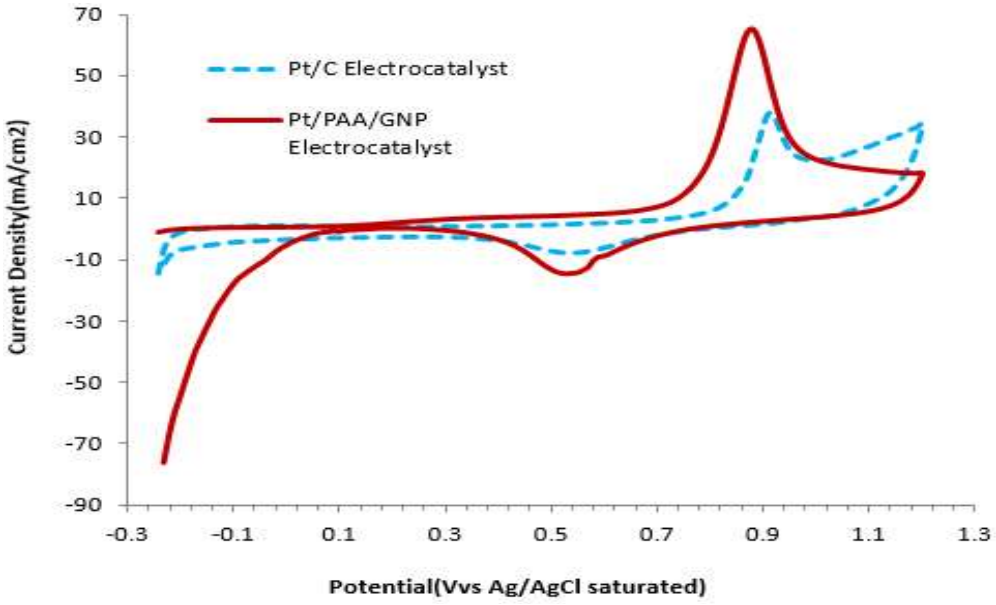

Fig. 12. CO stripping results for Pt/PAA/GNP and Pt/C electrocatalysts in 0.5M H_2SO_4solution, scan rate: 50mV s^{-1}

electro-oxidation of pre-adsorbed CO. The peak at about 0.89 V and 0.93V versus Ag/AgCl, represents the electro-oxidation of the irreversibly adsorbed CO on Pt/PAA/GNP and Pt/C, respectively.

The calculated peak charge Q_{CO}, is related to the reaction:

$$Pt\text{-}CO+H_2O \rightarrow Pt+CO_2+2e^-+2H^+ \quad (1)$$

the charge Q_{CO} ($mCcm^{-2}$) was used to compare the active surface area of the catalyst, calculated from the following equation:

$$ESA_{CO}=Q_{CO}/([Pt]\times 0.484) \quad (2)$$

Where the value 0.484 represents the charge density required to oxidize a monolayer of CO on bright Pt [77, 78] .

The ESA values calculated from the CO electro-oxidation area (ESA_{CO}) are 55.62 and 23.24 m^2g^{-1} for Pt/PAA/GNP and Pt/C, respectively. The higher ESA- CO of Pt/PAA/GNP catalyst indicates the higher Pt utilization in Pt/PAA/GNP. Therefore, the Pt/PAA/GNP electrocatalyst can contribute to the enhanced activity toward CO oxidation. Also, the electro-oxidation current of the CO ads species on the Pt/PAA/GNP is around 62.12$mAcm^{-2}$, which is much higher than that of Pt/C, indicating that the Pt/PAA/GNP electrocatalyst is more tolerant to CO poisoning than the Pt/C catalyst. There was one more interesting finding from the CO stripping study related to the CO electro-oxidation onset potential which can be further used to characterize the easiness of CO oxidation. The onset and peak potential of CO on Pt/PAA/GNP (0.56V, 0.89V) is much lower than that of Pt/C (0.67V, 0.93V), respectively, which suggest that the Pt/PAA/GNP electrocatalyst has a higher CO oxidation ability and improved activity.

Another interesting finding is the difference between desorption area values of H^+ and CO in the prepared catalysts. The ESA values from H^+ adsorption and CO stripping areas are listed in Table 3. As can be seen, the two ESA values are closer in the case of Pt/C for the Pt/PAA/GNP electrocatalysts; however, the ESA_{H+} is relatively larger than theESA_{CO} values.

Table 3 ESA values for electrodes from a H^+ adsorption and O desorption, respectively.

Electrode	ESA_{H+} m^2g^{-1}	ESA_{CO} m^2g^{-1}
Pt/ PAA/GNP	40.53	55.62
Pt/C	17.61	23.24

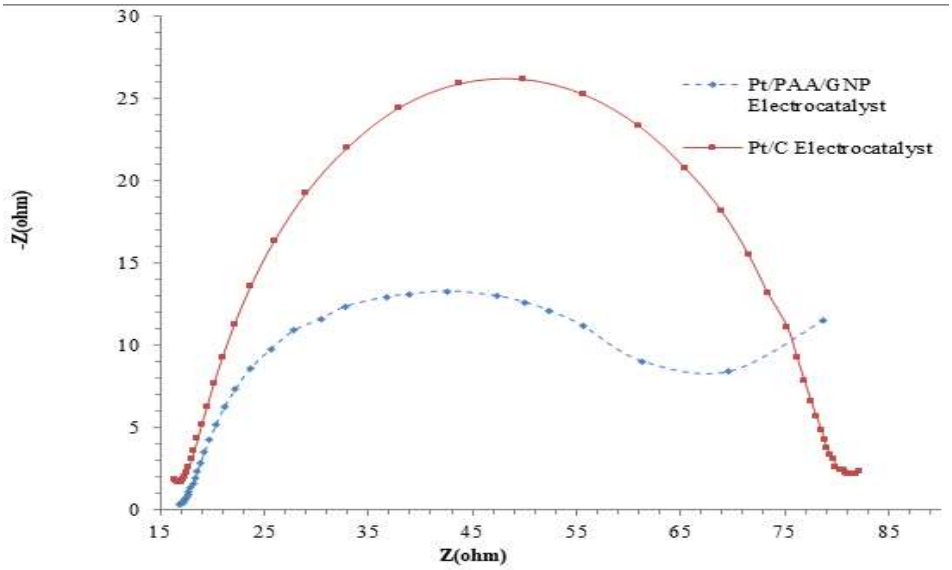

Fig. 13. Nyquist impedance spectra of Pt/C and Pt/ PAA/GNP in 0.5M H_2SO_4+1M CH_3 OH solution.

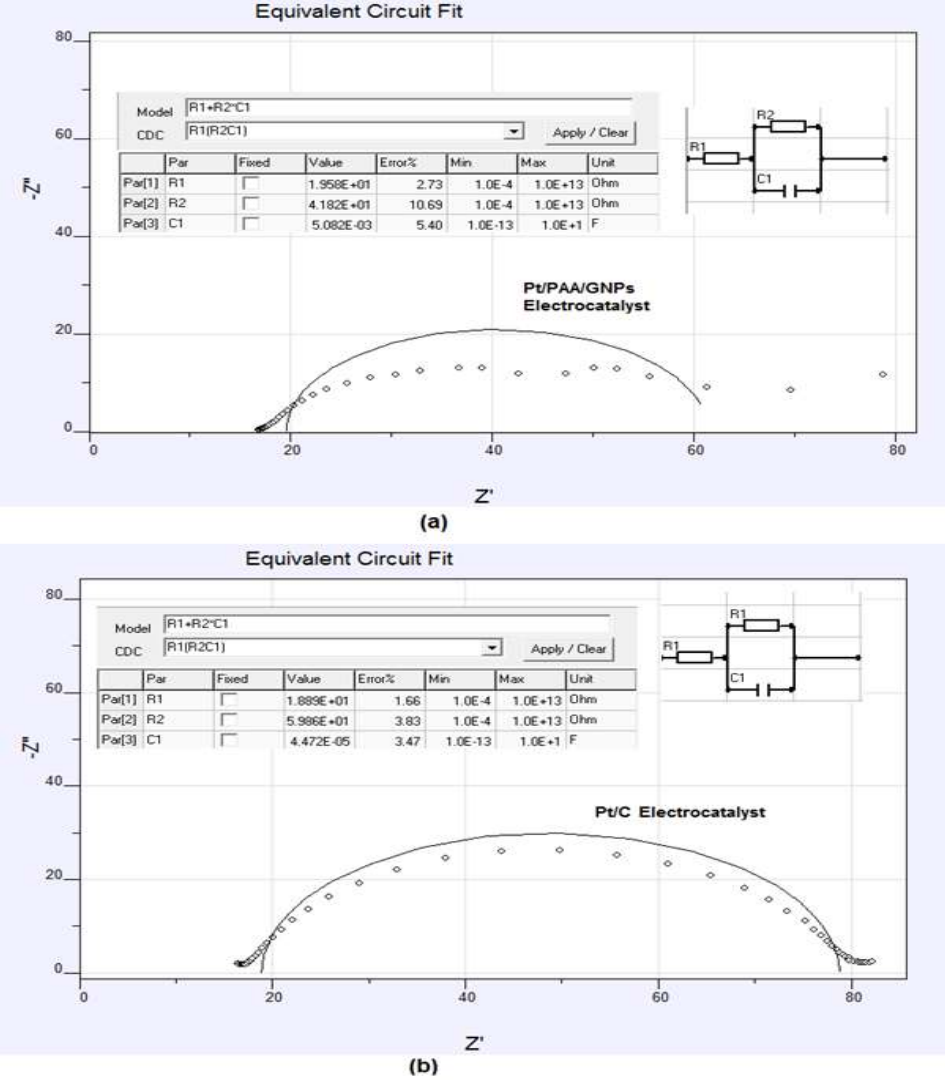

Fig. 14. Equivalent circuit of fitted EIS data of (a) Pt/PAA/GNP and (b) Pt/C in 0.5M H_2SO_4+1M CH_3 OH solution.

3.2.3 Electrochemical Impedance Spectroscopy (EIS) Studies of the Electrocatalysts

The electrochemical impedance spectroscopy (EIS) measurements of the samples were performed at a potential of 0.5V versus Ag/AgCl by sweeping frequencies over the range of 1 mHz to 100 KHz with 55 points/decade and an alternating sinusoidal signal of 5mV peak to peak. All electrochemical measurements were performed under 25 °C. Nyquist plots are shown in Fig. 13. As can be seen, both of the impedance spectra display similar characteristics, i.e., a semi-circle at the high frequency region whose diameter is associated with the charge transfer resistance indicating the catalytic activity for MOR. In this plot, the real axis intercept at high frequency was found to be independent of the electrodes and corresponds to the uncompensated resistance of the bulk electrolyte solution. Also, in this plot the diameter of the semi-circle in Pt/PAA/GNP electrocatalyst is small in comparison to the impedance spectra of the commercial Pt/C electrocatalyst. In the other words, the charge transfer resistance of the Pt/PAA/GNP electrocatalyst is much lower than that of the Pt/C electrocatalyst showing the high activity for MeOH oxidation. In this figure, a relatively small straight line with a slope of 1 (45 °) is related to the infinite diffusion at Pt/PAA/GNP electrocatalyst corresponding to the Warburge impedance at low frequency.

3.2.3.1 Equivalent circuit

The main features of the impedance measurements can be explained using the equivalent circuit from Fig. 14. This circuit contains the sum of electrode and electrolyte ohmic resistance (R1) and charge transfer resistance (R2), which controls the electron transfer kinetics of electroactive species at electrode interface parallel to constant phase element associated with double layer capacity (C1). The experimental impedance data are shown as an open diamond, while the solid line represents a theoretical fit obtained using an equivalent circuit model illustrated in scheme14. In this figure, the Randles equivalent circuit of fitted EIS data of Pt/C and Pt/ PAA/GNP are also presented along the values of R1, R2, and C1 of each electroctalyst. Ohmic resistance evaluated from the intercept of the x axis and the charge transfer resistance from the radius of semicircles.

3.2.4 Short term stability

Chronoamperometric experiments were performed

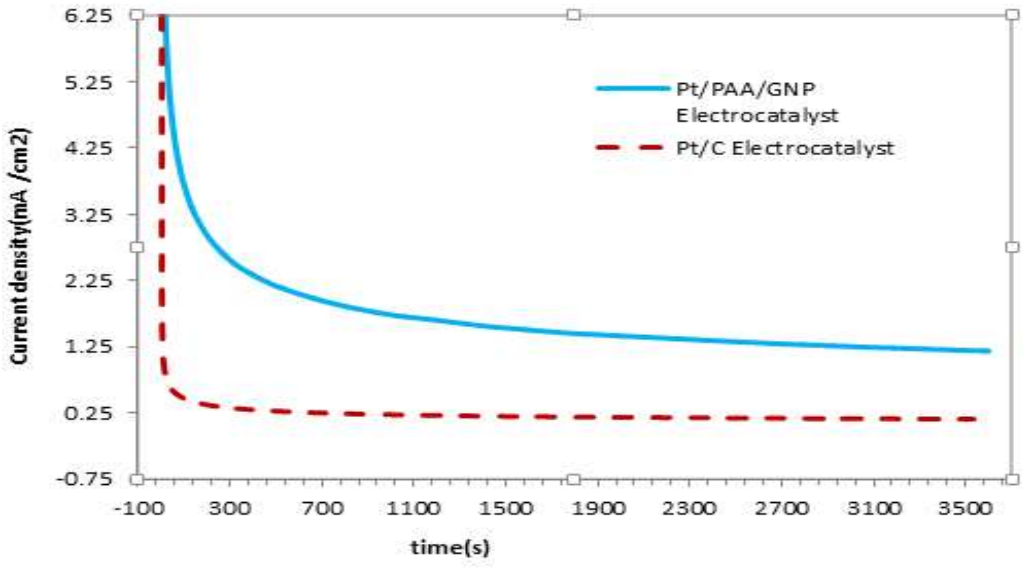

Fig. 15. Chronoamperometric curves of Pt/ PAA/GNP and Pt/C catalysts in N2 saturated aqueous solution of 0.5M H_2SO_4 containing 1M CH_3 OH at fixed potential of 0.4V for 1h.

to observe the stability and possible poisoning of the composite electrocatalyst under short time (1hour) continuous operation in 0.5M H_2SO_4+1M CH_3 OH at 0.4V(open circuit voltage). As seen from Fig. 15, the current density of the prepared Pt /GNP/ PAA electrocatalyst and commercial Pt/C decayed rapidly at the initial stage, which might be due to the formation of intermediate species during methanol oxidation such as CO_{ads} and CH_{ads}. The current gradually reached a relatively steady state after a brief transient period. It is clear from Fig.15 that the current density for the Pt /GNP/PAA electrocatalyst is much higher than that of Pt/C in a longer time, indicating PAA functionalized graphene nanoplates support can improve mechanical property like stiffness and strain strength [49], electrocatalytic activity, and stability of the composite. These results again confirm the high tolerance to the intermediate species and superior electrocatalytic performance of the prepared Pt/PAA/GNP nanocomposite catalyst in MOR.

Conclusion

In the present investigation, a Pt/PAA/GNP electrocatalyst was prepared by a microwave assisted polyol synthesis method and its physical and electrochemical properties with special characteristics were observed. These properties include a successful dispersion of catalyst nanoparticles on the support, higher CO electro-oxidation peak potential, much higher methanol electro-oxidation current density, and good stability in the presence of methanol in comparison to commercial Pt/C. These findings imply that Pt/PAA/GNP could be a promising catalyst for anode applications with superior activity and high methanol tolerance in high–performance DMFCs. The pulse-microwave procedure was adopted in order to avoid the agglomeration of metal particles at high temperatures. This is due to the fact that continuous microwave can easily cause a quite rapid heating rate for carbon materials. In this process, ethylene glycol acts not only as dispersant and reducing agent, but also as the microwave additive due to the fact that the dielectric constant and dielectric loss for ethylene glycol are high; and consequently, rapid heating takes place under the microwave radiation. The support, graphene, is also a microwave-sensitive material, which is believed to play an important role in the acceleration of the metal reduction. In conclusion, the present pulse-microwave assisted polyol method is simple, practical, and effective for the very rapid synthesis of a high dispersed high loading Pt-based electrocatalyst. The quite short metal reduction process is attractive and interesting from an economic point of view. Moreover, the as-prepared Pt/PAA/ GNP catalysts exhibited comparable electrocatalytic activity for the oxygen reduction reaction as the commercial catalyst.

Acknowledgement

This work was supported by Novel Technologies and the Hydrogen and Fuel cell Research Institute, Urmia University -Iran.

References

[1] Lamy C., Lima A., LeRhun V., Delime F., Coutanceau C. and Léger J.-M., "Recent advances in the development of direct alcohol fuel cells (DAFC)", J. Power Sources, 2002,105: 283.

[2] Zainoodin A., Kamarudin S.K. and Daud W.R.W., "Electrode in direct methanol fuel cells", Int. J. Hydrogen Energy, 2010,35: 4606.

[3] Evarts S.E., Kendrick I., Wallstrom B.L., Mion T., Abedi M., Dimakis N. and Smotkin E.S., "Ensemble site requirements for oxidative adsorption of methanol and ethanol on Pt membrane electrode assemblies", ACS Catal., 2012,2: 701.

[4] Jeon M.K., Lee K.R., Lee W.S., Daimon H., Nakahara A. and Woo S.I., "Investigation of Pt/WC/C catalyst for methanol electro-oxidation and oxygen electro-reduction", J. Power Sources, 2008,185: 927.

[5] Arico A., Srinivasan S. and Antonucci V., "DMFCs: from fundamental aspects to technology development", Fuel cells, 2001,1: 133.

[6] Vigier F., Coutanceau C., Perrard A., Belgsir E. and

Lamy C., "Development of anode catalysts for a direct ethanol fuel cell", J. Appl. Electrochem., 2004,34: 439.

[7] Qiu H. and Zou F., "Nanoporous PtCo surface alloy architecture with enhanced properties for methanol electrooxidation", ACS appl. mater. interfaces, 2012,4: 1404.

[8] Salgado J.R.C., Antolini E. and Gonzalez E.R., "Carbon supported Pt–Co alloys as methanol-resistant oxygen-reduction electrocatalysts for direct methanol fuel cells", Applied Catalysis B: Environmental, 2005,57: 283.

[9] Bong S., Kim Y.-R., Kim I., Woo S., Uhm S., Lee J. and Kim H., "Graphene supported electrocatalysts for methanol oxidation", Electrochem. Commun., 2010,12: 129.

[10] Li Y., Gao W., Ci L., Wang C. and Ajayan P.M., "Catalytic performance of Pt nanoparticles on reduced graphene oxide for methanol electro-oxidation", Carbon, 2010,48: 1124.

[11] Dong L., Gari R.R.S., Li Z., Craig M.M. and Hou S., "Graphene-supported platinum and platinum–ruthenium nanoparticles with high electrocatalytic activity for methanol and ethanol oxidation", Carbon, 2010,48: 781.

[12] Matsumoto T., Komatsu T., Arai K., Yamazaki T., Kijima M., Shimizu H., Takasawa Y. and Nakamura J., "Reduction of Pt usage in fuel cell electrocatalysts with carbon nanotube electrodes", Chem. Commun., 2004: 840.

[13] Yoo E., Okada T., Kizuka T. and Nakamura J., "Effect of carbon substrate materials as a Pt–Ru catalyst support on the performance of direct methanol fuel cells", J. Power Sources, 2008,180: 221.

[14] Liao S., Holmes K.-A., Tsaprailis H. and Birss V.I., "High performance PtRuIr catalysts supported on carbon nanotubes for the anodic oxidation of methanol", J.Am. Chem. Soc., 2006,128: 3504.

[15] Novoselov K.S., Geim A.K., Morozov S., Jiang D., Katsnelson M.I., Grigorieva I., Dubonos S., Firsov and AA, "Two-dimensional gas of massless Dirac fermions in graphene", Nature, 2005,438: 197.

[16] Zhang Y., Tan Y.-W., Stormer H.L. and Kim P., "Experimental observation of the quantum Hall effect and Berry's phase in graphene", Nature, 2005,438: 201.

[17] A.K. Geim K.S.N., "The rise of graphene", Nat. Mater, 2007,6: 183.

[18] Huang H., Chen H., Sun D. and Wang X., "Graphene nanoplate-Pt composite as a high performance electrocatalyst for direct methanol fuel cells", J. Power Sources, 2012,204: 46.

[19] Wang L., Tian C., Wang H., Ma Y., Wang B. and Fu H., "Mass production of graphene via an in situ self-generating template route and its promoted activity as electrocatalytic support for methanol electroxidization", J.Physical chem.C, 2010,114: 8727.

[20] Li Y., Tang L. and Li J., "Preparation and electrochemical performance for methanol oxidation of Pt/graphene nanocomposites", Electrochem. Commun., 2009,11: 846.

[21] Luo B., Xu S., Yan X. and Xue Q., "Graphene nanosheets supported hollow Pt&CoSn (OH) 6 nanospheres as a catalyst for methanol electro-oxidation", J. Power Sources, 2012,205: 239.

[22] Li D., Müller M.B., Gilje S., Kaner R.B. and Wallace G.G., "Processable aqueous dispersions of graphene nanosheets", Nat.Nanotechnol., 2008,3: 101.

[23] Park S., An J., Piner R.D., Jung I., Yang D., Velamakanni A., Nguyen S.T. and Ruoff R.S., "Aqueous suspension and characterization of chemically modified graphene sheets", Chem. Mater., 2008,20: 6592.

[24] Fan X., Peng W., Li Y., Li X., Wang S., Zhang G. and Zhang F., "Deoxygenation of exfoliated graphite oxide under alkaline conditions: a green route to graphene preparation", Adv. Mater., 2008,20: 4490.

[25] Park S., An J., Jung I., Piner R.D., An S.J., Li X., Velamakanni A. and Ruoff R.S., "Colloidal suspensions of highly reduced graphene oxide in a wide variety of organic solvents", Nano Lett., 2009,9: 1593.

[26] Chien C.-C. and Jeng K.-T., "Effective preparation of carbon nanotube-supported Pt–Ru electrocatalysts", Mater. Chem. Phys., 2006,99: 80.

[27] Lee K.R., Lee K.U., Lee J.W., Ahn B.T. and Woo S.I., "Electrochemical oxygen reduction on nitrogen doped graphene sheets in acid media", Electrochem. Commun., 2010,12: 1052.

[28] Li Y., Wang J., Li X., Geng D., Banis M.N., Li R. and Sun X., "Nitrogen-doped graphene nanosheets as cathode materials with excellent electrocatalytic activity for high capacity lithium-oxygen batteries", Electrochem. Commun., 2012,18: 12.

[29] Qu L., Liu Y., Baek J.-B. and Dai L., "Nitrogen-doped graphene as efficient metal-free electrocatalyst for oxygen reduction in fuel cells", ACS nano, 2010,4: 1321.

[30] Long D., Li W., Ling L., Miyawaki J., Mochida I. and Yoon S.-H., "Preparation of nitrogen-doped graphene sheets by a combined chemical and hydrothermal reduction of graphene oxide", Langmuir, 2010,26: 16096.

[31] Shao Y., Zhang S., Wang C., Nie Z., Liu J., Wang Y. and Lin Y., "Highly durable graphene nanoplatelets supported Pt nanocatalysts for oxygen reduction", J. Power Sources, 2010,195: 4600.

[32] Shi Q. and Mu S., "Preparation of Pt/poly (pyrogallol)/ graphene electrode and its electrocatalytic activity for methanol oxidation", J. Power Sources, 2012,203: 48.

[33] Wang H., Hao Q., Yang X., Lu L. and Wang X., "Graphene oxide doped polyaniline for supercapacitors", Electrochem. Commun., 2009,11: 1158.

[34] Gómez H., Ram M.K., Alvi F., Villalba P., Stefanakos E.L. and Kumar A., "Graphene-conducting polymer nanocomposite as novel electrode for supercapacitors", J. Power Sources, 2011,196: 4102.

[35] Zhao Y., Zhan L., Tian J., Nie S. and Ning Z., "Enhanced electrocatalytic oxidation of methanol on Pd/ polypyrrole–graphene in alkaline medium", Electrochim. Acta, 2011,56: 1967.

[36] Wang J., Xu Y., Zhu J. and Ren P., "Electrochemical in situ polymerization of reduced graphene oxide/ polypyrrole composite with high power density", J. Power Sources, 2012,208: 138.

[37] Wietecha M.S., Zhu J., Gao G., Wang N., Feng H., Gorring M.L., Kasner M.L. and Hou S., "Platinum nanoparticles anchored on chelating group-modified graphene for methanol oxidation", J. Power Sources, 2012,198: 30.

[38] Yang S.-Y., Chang K.-H., Lee Y.-F., Ma C.-C.M. and Hu C.-C., "Constructing a hierarchical graphene–carbon nanotube architecture for enhancing exposure of graphene and electrochemical activity of Pt nanoclusters", Electrochem. Commun., 2010,12: 1206.

[39] Jha N., Jafri R.I., Rajalakshmi N. and Ramaprabhu S., "Graphene-multi walled carbon nanotube hybrid electrocatalyst support material for direct methanol fuel cell", Int. J. Hydrogen Energy, 2011,36: 7284.

[40] Paul R.K. and Mulchandani A., "Platinum nanoflowers decorated three-dimensional graphene–carbon nanotubes hybrid with enhanced electrocatalytic activity", J. Power Sources, 2013,223: 23.

[41] Mai Y., Shi S., Zhang D., Lu Y., Gu C. and Tu J., "NiO–graphene hybrid as an anode material for lithium ion batteries", J. Power Sources, 2012,204: 155.

[42] Williams G., Seger B. and Kamat P.V., "TiO2-graphene nanocomposites. UV-assisted photocatalytic reduction of graphene oxide", ACS nano, 2008,2: 1487.

[43] Cheng P., Yang Z., Wang H., Cheng W., Chen M., Shangguan W. and Ding G., "TiO 2–graphene nanocomposites for photocatalytic hydrogen production from splitting water", Int. J. Hydrogen Energy, 2012,37: 2224.

[44] Taladriz-Blanco P., Rodríguez-Lorenzo L., Sanles-Sobrido M., Hervés P., Correa-Duarte M.A., Alvarez-Puebla R.A. and Liz-Marzán L.M., "SERS study of the controllable release of nitric oxide from aromatic nitrosothiols on bimetallic, bifunctional nanoparticles supported on carbon nanotubes", ACS appl. mater. interfaces, 2008,1: 56.

[45] Grzelczak M., Correa-Duarte M.A., Salgueiriño-Maceira V., Rodríguez-González B., Rivas J. and Liz-Marzán L.M., "Pt-Catalyzed Formation of Ni Nanoshells on Carbon Nanotubes", Angew. Chem. Int. Ed., 2007,46: 7026.

[46] Olek M., Hilgendorff M. and Giersig M., "A simple route for the attachment of colloidal nanocrystals to noncovalently modified multiwalled carbon nanotubes", Colloids Surf., A, 2007,292: 83.

[47] Tóháti H.M., Botka B., Németh K., Pekker Á., Hackl R. and Kamarás K., "Infrared and Raman investigation of carbon nanotube-polyallylamine hybrid systems", physica status solidi (b), 2010,247: 2884.

[48] Park S., Dikin D.A., Nguyen S.T. and Ruoff R.S., "Graphene oxide sheets chemically cross-linked by polyallylamine", J.Physical chem.C, 2009,113: 15801.

[49] Satti A., Larpent P. and Gun'ko Y., "Improvement of mechanical properties of graphene oxide/poly (allylamine) composites by chemical crosslinking", Carbon, 2010,48: 3376.

[50] Fu Y.-P., Chang Y.-S. and Wen S.-B., "Microwave-induced combustion synthesis and electrical conductivity of Ce1− xGdxO2− 1/2x ceramics", Mater. Res. Bull., 2006,41: 2260.

[51] H.M. Kingston S.J.H., "Microwave-Enhanced

Chemistry", American Chemical Society, Washington, DC, 2005.

[52] Bonet F., Delmas V., Grugeon S., Urbina R.H., Silvert P. and Tekaia-Elhsissen K., "Synthesis of monodisperse Au, Pt, Pd, Ru and Ir nanoparticles in ethylene glycol", Nanostruct. Mater., 1999,11: 1277.

[53] Saini P., Khobaib G., Singh M., Tandon R.P., Singh S. and Mahapatro A.K., "Functionalization of polyallylamine on graphene oxide", Adv Mater Proceed, 2017,2: 209.

[54] Kim Y.-K. and Min D.-H., "Simultaneous reduction and functionalization of graphene oxide by polyallylamine for nanocomposite formation", Carbon letters, 2012,13: 29.

[55] Saini P., Singh M., Singh S.P. and Mahapatro A.K., "Spectroscopic and electronic properties of polyallylamine functionalized graphene oxide films", Vacuum, 2018,154: 110.

[56] Wang G., Shen X., Wang B., Yao J. and Park J., "Synthesis and characterisation of hydrophilic and organophilic graphene nanosheets", Carbon, 2009,47: 1359.

[57] Soin N., Roy S.S., Lim T.H. and McLaughlin J.A., "Microstructural and electrochemical properties of vertically aligned few layered graphene (FLG) nanoflakes and their application in methanol oxidation", Mater. Chem. Phys., 2011,129: 1051.

[58] Wu Z.-S., Ren W., Gao L., Liu B., Jiang C. and Cheng H.-M., "Synthesis of high-quality graphene with a pre-determined number of layers", Carbon, 2009,47: 493.

[59] Morrison R. and Boyd R., "Organic Chemistry, 6th", Englewood Cliffs, NJ: Prentice Hall, 1992.

[60] Nakamoto K. and Nakamoto K., "Infrared and Raman spectra of inorganic and coordination compounds", Wiley. 1977.

[61] D'Urso L., Compagnini G., Puglisi O., Scandurra A. and Cataliotti R.S., "Vibrational and photoelectron investigation of amorphous fluorinated carbon films", J.Physical chem.C, 2007,111: 17437.

[62] Park S. and Ruoff R.S., "Chemical methods for the production of graphenes", Nat.Nanotechnol., 2009,4: 217.

[63] Stankovich S., Piner R.D., Chen X., Wu N., Nguyen S.T. and Ruoff R.S., "Stable aqueous dispersions of graphitic nanoplatelets via the reduction of exfoliated graphite oxide in the presence of poly (sodium 4-styrenesulfonate)", J. Mater. Chem., 2006,16: 155.

[64] Stankovich S., Dikin D.A., Piner R.D., Kohlhaas K.A., Kleinhammes A., Jia Y., Wu Y., Nguyen S.T. and Ruoff R.S., "Synthesis of graphene-based nanosheets via chemical reduction of exfoliated graphite oxide", Carbon, 2007,45: 1558.

[65] Hassan H.M., Abdelsayed V., Abd El Rahman S.K., AbouZeid K.M., Terner J., El-Shall M.S., Al-Resayes S.I. and El-Azhary A.A., "Microwave synthesis of graphene sheets supporting metal nanocrystals in aqueous and organic media", J. Mater. Chem., 2009,19: 3832.

[66] Ferrari A.C., "Raman spectroscopy of graphene and graphite: disorder, electron–phonon coupling, doping and nonadiabatic effects", Solid State Commun., 2007,143: 47.

[67] Berciaud S., Ryu S., Brus L.E. and Heinz T.F., "Probing the intrinsic properties of exfoliated graphene: Raman spectroscopy of free-standing monolayers", Nano Lett., 2008,9: 346.

[68] Dresselhaus M.S., Jorio A., Hofmann M., Dresselhaus G. and Saito R., "Perspectives on carbon nanotubes and graphene Raman spectroscopy", Nano Lett., 2010,10: 751.

[69] Ferrari A.C. and Robertson J., "Interpretation of Raman spectra of disordered and amorphous carbon", Physical review B, 2000,61: 14095.

[70] Kim Y.-K. and Min D.-H., "Preparation of the hybrid film of poly (allylamine hydrochloride)-functionalized graphene oxide and gold nanoparticle and its application for laser-induced desorption/ionization of small molecules", Langmuir, 2012,28: 4453.

[71] Culity B. and Stock S., "Elements of X-ray Diffraction", Edison Wesley, London, 1978.

[72] Kong B.-S., Yoo H.-W. and Jung H.-T., "Electrical conductivity of graphene films with a poly (allylamine hydrochloride) supporting layer", Langmuir, 2009,25: 11008.

[73] Shao Y., Sui J., Yin G. and Gao Y., "Nitrogen-doped carbon nanostructures and their composites as catalytic materials for proton exchange membrane fuel cell", Applied Catalysis B: Environmental, 2008,79: 89.

[74] Shao Y., Sui J., Yin G. and Gao Y., "Nitrogen-doped carbon nanostructures and their composites as catalytic materials for proton exchange membrane fuel cell", Appl. Catal.B., 2008,79: 89.

[75] Sumpter B.G., Meunier V., Romo-Herrera J.M.,

Cruz-Silva E., Cullen D.A., Terrones H., Smith D.J. and Terrones M., "Nitrogen-mediated carbon nanotube growth: diameter reduction, metallicity, bundle dispersability, and bamboo-like structure formation", ACS nano, 2007,1: 369.

[76] Honda K., Yoshimura M., Rao T.N., Tryk D., Fujishima A., Yasui K., Sakamoto Y., Nishio K. and Masuda H., "Electrochemical properties of Pt-modified nano-honeycomb diamond electrodes", J. Electroanal. Chem., 2001,514: 35.

[77] Ciureanu M. and Wang H., "Electrochemical Impedance Study of Electrode-Membrane Assemblies in PEM Fuel Cells: I. Electro-oxidation of H 2 and H 2/ CO Mixtures on Pt-Based Gas-Diffusion Electrodes", J. Electrochem. Soc., 1999,146: 4031.

[78] Weaver M., Chang S.-C., Leung L.-W., Jiang X., Rubel M., Szklarczyk M., Zurawski D. and Wieckowski A., "Evaluation of absolute saturation coverages of carbon monoxide on ordered low-index platinum and rhodium electrodes", J. Electroanal. Chem., 1992,327: 247.